Mechanics of membrane-cytoskeleton attachment in Paramecium

Clément Campillo, Julie Jerber, Cathy Fisch, Maria Simoes-Betbeder, Pascale Dupuis-Williams, Pierre Nassoy, C. Sykes

Mechanics of membrane–cytoskeleton attachment in *Paramecium*

2012 New J. Phys. 14 125016

(http://iopscience.iop.org/1367-2630/14/12/125016)

New Journal of Physics
The open access journal for physics

Mechanics of membrane–cytoskeleton attachment in *Paramecium*

C Campillo[1,2,3], J Jerber[4], C Fisch[5], M Simoes-Betbeder[6], P Dupuis-Williams[5,7,8], P Nassoy[1,2,3] and C Sykes[1,2,3,8]

[1] Institut Curie, Centre de Recherche, Laboratoire Physico-Chimie, Paris F-75248, France
[2] CNRS, UMR168, Paris F-75248, France
[3] Université Paris 6, Paris F-75248, France
[4] CNRS, UMR 5534, Université Lyon 1, F-69622 Villeurbanne Cedex, France
[5] INSERM UMR-S 757 Université Paris Sud, France
[6] CNRS UMR 7633, Centre des Matériaux de l'ENSMP-ARMINES, F-91003 Evry Cedex, France
[7] Ecole Supérieure de Physique et Chimie Industrielles, Paris, France
E-mail: pascale.dupuis-williams@u-psud.fr and cecile.sykes@curie.fr

New Journal of Physics **14** (2012) 125016 (9pp)
Received 17 August 2012
Published 19 December 2012
Online at http://www.njp.org/
doi:10.1088/1367-2630/14/12/125016

Abstract. In this paper we assess the role of the protein MKS1 (Meckel syndrome type 1) in the cortical membrane mechanics of the ciliated protist *Paramecium*. This protein is known to be crucial in the process of cilium formation, and we investigate its putative role in membrane–cytoskeleton attachment. Therefore, we compare cells where the gene coding for MKS1 is silenced to wild-type cells. We found that scanning electron microscopy observation of the cell surface reveals a cup-like structure in wild-type cells that is lost in silenced cells. Since this structure is based on the underlying cytoskeleton, one hypothesis to explain this observation is a disruption of membrane attachment to the cytoskeleton in the absence of MKS1 that should affect plasma membrane mechanics. We test this by probing the mechanics of wild-type and silenced cells by micropipette aspiration. Strikingly, we observe

[8] Authors to whom any correspondence should be addressed.

that, at the same aspiration pressure, the membrane of silenced cells is easily aspirated by the micropipette whereas that of wild-type cells enters only at a moderate velocity, an effect that suggests a detachment of the membrane from the underlying cytoskeleton in silenced cells. We quantify this detachment by measuring the deformation of the cell cortex and the rate of cell membrane entry in the micropipette. This study offers a new perspective for the characterization of membrane–cytoskeleton attachment in protists and paves the way for a better understanding of the role of membrane–cortex attachment in cilium formation.

S Online supplementary data available from stacks.iop.org/NJP/14/125016/mmedia

Contents

1. Introduction

Cilia are membrane-covered microtubular structures, which are evolutionarily conserved from protists to humans. Among the proteins that are important for correct cilia formation and stability are those containing the B9 domain, whose impairment causes severe human developmental disorders [1]. In the absence of B9 domain proteins, cilia are absent, fewer or shorter, depending on the cell type [2–7], and their sensory functions are defective. *Paramecium*, with its about 5000 cilia, is a suitable model organism for studying cilium formation and stability. *Paramecium* is a protist whose shape is ellipsoidal with a length and a width of about 100 and 40 μm, respectively. It swims at a velocity of about 1 mm s^{-1} through the beating of its cilia which are connected to an underlying rigid cytoskeleton made of epiplasmin [8] and actin [9]. Structural analysis in *Paramecium* suggests that the B9 domain proteins have a role in the attachment of the membrane to the cytoskeleton [10]. The aim of this paper is to verify this hypothesis. Therefore, we measure the mechanical properties of the cell surface by micropipette aspiration in wild-type *Paramecia* and cells where the gene Meckel syndrome type 1 (MKS1), coding for one of the B9 domain proteins, is silenced by RNA interference (RNAi). RNAi is a conserved biological process of post-transcriptional gene silencing. This process relies on the

degradation of a specific messenger RNA triggered by the introduction of small homologous double stranded-RNAs (called small interfering RNAs or siRNAs) in a cell.

First, we observe by scanning electron microscopy in silenced cells the loss of the cup-like structure of the cell surface, suggesting the detachment of the membrane from the underlying cytoskeleton. To characterize the mechanics of the cell surface, two techniques are currently adaptable to cells: membrane nanotube extrusion [11] and micropipette aspiration that was used on outer hair cells [12] and *Dictyostelium* [13]. However, only micropipette aspiration can be performed on *Paramecium* because of the presence of beating cilia that prevent membrane accessibility for nanotube pulling. We thus use micropipette aspiration to compare the plasma membrane mechanical responses of wild-type and MKS1 silenced cells. To our knowledge, this is the first study of the mechanical response of the *Paramecium* membrane. We found that both in wild-type and in silenced cells, at a fixed aspiration pressure, the membrane detaches visibly from the underlying cytoskeleton after about 10 s. Subsequently, the membrane and cytoskeleton progress in the micropipette at different velocities. However, silenced and wild-type cells drastically differ in the amount of membrane that can be pulled in the micropipette at a given time: pulling the membrane of silenced cells is easier than pulling that of wild-type cells. We found that while the membrane surface pulled from a wild-type cell is limited to the micropipette area, the aspirated membrane surface is limited to silenced cells. These results reveal that the resistance to flow in the micropipette of the wild-type cell membrane is lost in MKS1 silenced cells, likely due to the lack of attachment to the underlying cytoskeleton in these mutant cells. Our study strongly supports the hypothesis that the B9 domain proteins are crucial for membrane–cytoskeleton attachment.

2. Materials and methods

2.1. Strains and culture conditions

Wild-type cells of stock d4-2 are a derivative of the wild-type stock 51 of *Paramecium tetraurelia*. Cells were grown at 27 °C in *Paramecium* culture medium: a buffered infusion of wheat grass powder (l'Arbre de vie, Luçay le Male, France), supplemented with 0.4 μg ml^{-1} β-sitosterol and inoculated with non-pathogenic *Klebsiella pneumoniae*.

2.2. Gene silencing in Paramecium tetraurelia

The sequence of MKS1 (GSPATP00011904001) is cloned between two T7 promoters in the L4440 feeding vector modified with the Gateway® vector conversion system (Invitrogen). The construct is used for transformation of an RNase III-deficient strain of *Escherichia coli* with an IPTG-inducible T7 polymerase, HT115 (DE3). Paramecia are cultured in double-stranded RNA-expressing bacteria as previously described and maintained at a cell density of 20 paramecia per ml. Throughout the experiment, paramecia are sub-cloned daily and re-fed with freshly induced bacteria to maintain the RNAi effect; cells are used at 48–72 h after phenotypic screening. Control cells are grown under the same conditions with HT115 bacteria carrying no plasmid.

2.3. Scanning electron microscopy

For scanning electron microscopy, cells are washed in 10 mM Tris, pH 7.4, fixed overnight with 2.5% glutaraldehyde in 0.05 M cacodylate buffer (pH 7.3) and then washed and

post-fixed in 0.4% OsO_4 for 1 h. After dehydration, samples are critical-point dried (Emitech K850) and coated with gold (Jeol JFC-1200). Samples were visualized with a Jeol 840A scanning microscope.

Alternatively, cells are washed in the culture medium buffer BHB (4.75 mM Tris HCl, 10.56 mM disodium phosphate and 0.94 mM monosodium phosphate), fixed overnight with 2% glutaraldehyde in BHB and then washed and post-fixed in 1% OsO_4 for 1 h. After dehydration with a graded series of ethanol, samples are chemically dried with HMDS (hexamethyldisilazane; VWR) and sputter coated with gold–palladium (Cressington Sputter Coater 208HR) before visualization with a Zeiss Gemini DSM 982 scanning microscope.

2.4. Micropipette aspiration

The observation chamber, composed of two glass coverslips separated by a Parafilm spacer, is placed on the stage of an inverted microscope (Axiovert 200; Zeiss) equipped with a 100× immersion oil objective (Neofluar 1.3 NA). The chamber is filled with *Paramecium* culture medium. A glass micropipette, pulled from borosilicate capillaries (0.7/1.0 mm inner/outer diameter, Kimble, Vineland, NJ) with a laser puller (Sutter P2000) and microforged (DMF1000, World Precision Instruments, Aston, UK) to a radius of 3–4 μm, is inserted into the chamber. The aspiration pressure is adjusted by controlling the height of a mobile water tank connected to the micropipette. Transmission bright-field images are collected by a charge coupled device camera (XC-ST70CE, Sony, Japan) and recorded at 25 frames per second with a frame grabber (Picolo Pro 2) after contrast enhancement (Argus Image Processor; Hamamatsu, Japan). Image analysis is performed using a Matlab routine that semi-automatically detects and measures the morphology and length of the cell portion (or tongue) aspirated inside the micropipette.

3. Results

3.1. Effect of Meckel syndrome type 1 knockdown on the shape of Paramecium *plasma membrane*

In this section, we present scanning electron microscopy observation of the plasma membrane in wild-type and silenced *Paramecium*. The plasma membrane of *Paramecia* is structured through its attachment to the cortical cytoskeleton, organized into pits (dark gray, figures 1(a) and (b)) centered around one or two ciliated basal bodies and an endocytotic site [14]. The bottom of the cup is formed by a cytoskeleton of the family of intermediate filaments underlying the membrane [8]. The elevated ridges of the cup are delineated by cytoskeletal networks [14] including actin [15]. In MKS1 silenced cells (figure 1(c)), the surface of the cell is much flatter and the cortical units whose ridges are identifiable by the membrane folds have lost their typical cup-shaped relief. In conclusion, we observe a disappearance of the cup-like shape of the membrane in silenced cells. Note that we observe an intact cytoskeleton by phase contrast microscopy in silenced cells (see below), suggesting that the organization of the cortical cytoskeleton is unaffected by MKS1 silencing. As a consequence, the effect observed in figures 1(a) and (c) can be attributed to a detachment of the membrane from the cytoskeleton in silenced cells, as confirmed by the presence of numerous blebs (figure 1(c)), which are a hallmark of membrane–cytoskeleton dissociation. In support of this hypothesis, and since no means are available to specifically disrupt the links between the membrane and cytoskeleton in *Paramecium*, the treatment of cells with anti-actin drugs such as phalloïdin led to the

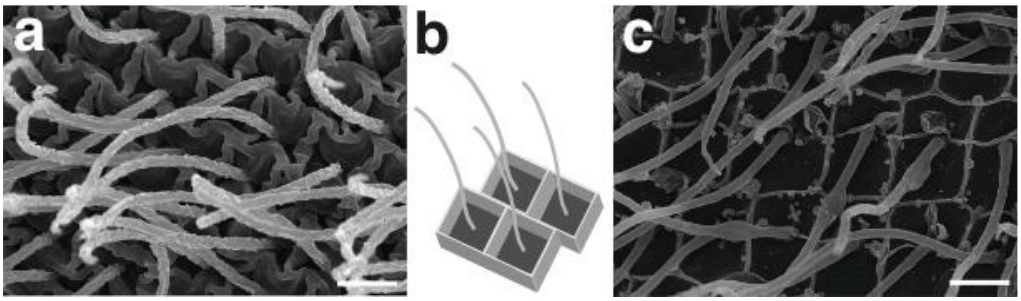

Figure 1. Scanning electron microscopy images of the *Paramecium* membrane for (a) a wild-type cell showing the pit structure of the membrane schemed in (b), and (c) a silenced cell showing the disruption of pits. Scale bar, 1 μm.

same phenotype of swelling, suggestive of membrane/actin disruption observed for MKS1 silenced cells.

3.2. Micropipette aspiration experiments

Scanning electron microscopy observations suggest a detachment of the plasma membrane from the cytoskeleton in silenced cells, which we further probe by micropipette aspiration. Previous micropipette studies on other cell types were performed on immobile cells, whereas here *Paramecia* keep their ability to move during the measurement. Therefore, in order to monitor cellular deformations, cells need to be immobilized through an aspiration force that overcomes the motility force [16, 17]. The swimming force of *Paramecium* reads $f_{\mathrm{swim}} = 3\pi\eta(4a + b/5)v$, where η is the water viscosity (10^{-3} Pa s), a and b are the width and length of *Paramecium* (40 and 100 μm), respectively, and v is its swimming speed (1 mm s^{-1}), leading to an estimate of 50 nN. The aspiration force is $f_{\mathrm{aspi}} = \pi R_{\mathrm{p}}^2 \Delta P$ with R_{p} the pipette radius (3 μm) and ΔP the aspiration pressure. Using values of ΔP of the order of 1–2 kPa, the aspiration force is 30–60 nN and allows both correct handling of cells and cell deformation (figures 2(a)–(c)). Note that for aspiration pressures lower than 1 kPa, we frequently observe the escape of *Paramecium* from the micropipette, which is consistent with the above-mentioned estimate for the minimal aspiration force.

During an aspiration experiment, the cell partially enters the micropipette and forms a tongue of length L that elongates with time (figure 2(a)). This phase is short (about 15 s) and is quickly followed by the detachment of the plasma membrane from its underlying cytoskeleton inside the micropipette for both control and silenced cells. First, we observe blebs that are smaller than the micropipette diameter (figure 2(b)). This happens at a time τ_1 after starting to aspirate in the micropipette. Then these blebs grow during about 10 s until they entirely fill the micropipette at time τ_2. After that time, two distinct interfaces can be tracked: the cell cortex (CC) and the cell membrane (CM) (figure 2(c)). A careful analysis of characteristic times reveals that times τ_1 and τ_2 are shorter for a higher aspiration pressure (2 kPa instead of 1 kPa) but no clear time difference is observed between wild-type and silenced cells (figure 2(d)). Both CC and CM interfaces progress inside the pipette and their distance increases with time for control and for silenced cells (figure 2(e)). In 50% of the cases, the aspirated membrane eventually breaks into a distinct cylindrical vesicle as observed earlier in outer hair cells [18] that remains connected through a membrane nanotether and is able to re-incorporate into the

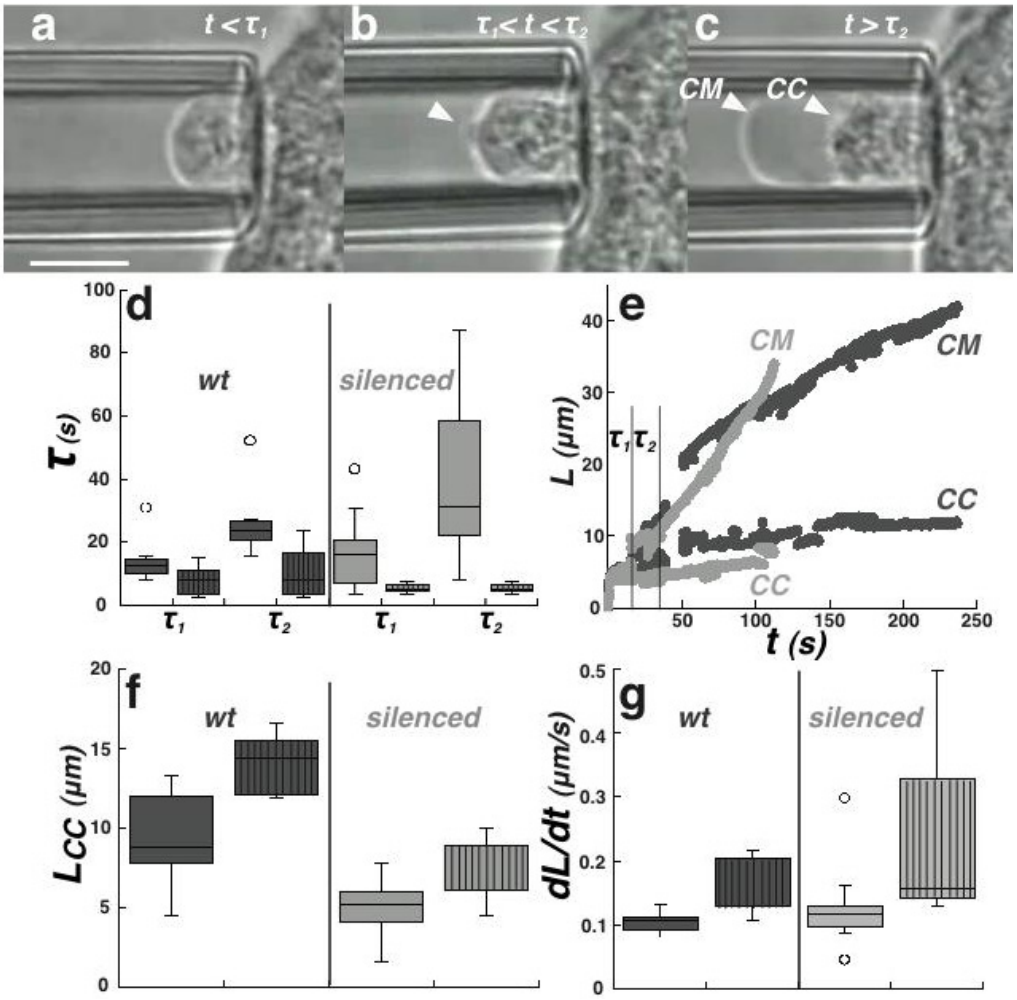

Figure 2. Micropipette aspiration of *Paramecium*. (a–c) Aspiration of a wild-type cell. (a) Initial simultaneous deformation of CM and CC, (b) initiation of a membrane bleb (white arrow) and (c) after bleb growth, two interfaces are tracked inside the micropipette: CC and CM. Scale bar, 5 μm. (d–g) Data for wild-type (dark gray) and silenced (light gray) cells, with aspiration pressure 1 kPa (plain boxes) or 2 kPa (hatched boxes). (d) Measured times for bleb nucleation τ_1 and bleb filling the micropipette τ_2. (e) Typical aspiration curves showing the progression of CC and CM with aspiration pressure 1 kPa. (f) Plateau tongue length of CC; (g) rate of CM entry inside the micropipette measured 100 s after bleb nucleation.

plasma membrane upon aspiration pressure release (supplementary figure S1, available from stacks.iop.org/NJP/14/125016/mmedia).

The variation of CC and CM tongue lengths in the micropipette (figure 2(e)) is a characteristic of the mechanical response of cells we monitor. Remarkably, the position of CC reaches a pseudo-plateau for both wild-type and silenced cells (figure 2(e)). The value of this plateau is always lower in silenced cells compared to wild-type cells (figure 2(f)). Contrastingly, we observe that the dynamics of CM in control and silenced cells are drastically different. The

growth of the CM tongue always slows down for wild-type cells ($N = 15$), while for silenced cells ($N = 16$), CM continuously flows inside the pipette at constant speed. More quantitatively, we show that the maximal slope of $L(t)$ for CM of control cells after a time longer than $\tau_2(100\,\mathrm{s})$ is significantly smaller than that (which is constant) for silenced cells (figure 2(g)). In conclusion, pulling out the membrane from wild-type cells is limited, whereas in silenced cells, there is no resistance to the pulling out of the membrane.

4. Discussion

There are two major features that distinguish silenced cells from wild-type cells: the cup-like shape of the cell surface that vanishes, and the capacity of the membrane to steadily enter the micropipette. Why is there less resistance against pulling the membrane of silenced cells, and how does it correlate to the membrane geometry alteration? Since the cortical cytoskeleton appears to be unchanged and the membrane is not disrupted, this implies that membrane–cytoskeleton attachment is affected by MKS1 silencing. In fact, the wild-type *Paramecium* membrane is made of pit-like corrugations where the membrane covers the underlying cytoskeleton; thus the 'real' surface largely exceeds its projected surface, as seen in figure 1(a). An estimate of this surface excess can be obtained considering that the pits are square-based boxes of $1.5\,\mu$m width and $1\,\mu$m height. The projected surface of a pit is $2.25\,\mu\mathrm{m}^2$ but its real membrane surface is $8.25\,\mu\mathrm{m}^2$, and then membrane detachment in a single pit releases $6\,\mu\mathrm{m}^2$ of membrane area. This area has to be compared with the membrane surface excess aspirated in the micropipette. For the control cell of figure 2(e), the surface of the dissociated membrane is about $540\,\mu\mathrm{m}^2$ (the difference between CC and CM positions is about $30\,\mu$m in a $3\,\mu$m radius pipette), which corresponds to the unfolding of 90 membrane pits. On the other hand, let us estimate the area of the cytoskeletal scaffold surface from the CM plateau in figure 2(e): the length of CC in the micropipette is about $10\,\mu$m, which leads to a surface area of about $180\,\mu\mathrm{m}^2$. This area corresponds to about 80 pits. These two separate estimates provide the same number of pits; thus the membrane surface that has been pulled in the micropipette corresponds to the unfolding of all pits trapped in the micropipette. As a consequence, in wild-type cells, the force exerted on the membrane by micropipette aspiration is only able to detach locally the membrane from its underlying cytoskeleton. In contrast, for silenced cells, the length of the membrane in the pipette continuously increases and rapidly outreaches the value of control cells in about 100 s. This indicates that in silenced cells, the huge increase of membrane surface in the micropipette can only be explained by the available membrane outside the micropipette, whose flow inside the pipette requires very little mechanical work. Moreover, in silenced cells, the deformation of the cortex is always smaller than in wild-type cells in the same pressure conditions (figures 2(e) and (f)), indicating that membrane deformation is easier in silenced cells since its effect on cortex deformation is smaller. Altogether, these results confirm the observation by scanning electron microscopy of silenced cells where the membrane seems detached from the cytoskeleton in the bottom of the pits. In conclusion, the membrane is more prone to detach in silenced cells than in control cells, confirming our hypothesis that adhesion between the cytoskeleton and the membrane is decreased in silenced cells. Moreover, the shorter cilia observed for silenced cells might indicate that the base is unsheathed in membrane, leading to cilia that appear shorter.

An estimate of the adhesion energy between the membrane and its underlying cytoskeleton could be obtained with the same aspiration technique than in outer hair cells [18] through

applying a variable aspiration pressure on the cell interface. The threshold value of the aspiration pressure at which the membrane detaches from its underlying cortex provides a quantitative measurement of the adhesion energy. In the case of *Paramecium*, which are swimming and can escape when aspired at low pressure, we could not probe the threshold pressure for membrane detachment. However, an alternative model to explain membrane flow in a comparable situation is based notably on a decrease of membrane–cytoskeleton attachment [19], in line with our assertion that the difference between wild-type and silenced cells reflects a lower density of membrane–cortex attachment. To further quantitatively characterize this membrane–cytoskeleton detachment, we can analyze the rate at which CM enters the micropipette (figure 1(g) and slopes of the curves of figure 1(e)). Adapting the framework developed by Evans and Needham [20] for the entry of lipid vesicles inside a pipette, we obtain that the rate of tongue entry is given by

$$\frac{\mathrm{d}L}{\mathrm{d}t} = \frac{\Delta P R_\mathrm{p}^2}{4\eta_S(1-(R_\mathrm{p}^2/R_\mathrm{v}^2)}, \tag{1}$$

where R_v is the radius of the vesicle and R_p is the radius of the micropipette. In our case $R_\mathrm{p}/R_\mathrm{v} = 1$ and we obtain an effective viscosity

$$\eta_\mathrm{eff} = \frac{\Delta P R_\mathrm{p}^2}{4\,(\mathrm{d}L/\mathrm{d}t)}. \tag{2}$$

Note that here η_eff reflects the interaction of the membrane with the cortex at which it is attached at long-range scale rather than the intrinsic viscosity of the lipid membrane, which is of the order of 10^{-8}–$10^{-7}\,\mathrm{N\,s\,m^{-1}}$ [21]. From figure 2(g) and equation (2) we derive that η_eff is smaller for silenced ($\eta_\mathrm{eff} = 0.10\,\mathrm{N\,s\,m^{-1}} \pm 0.05$ SD) than for wild-type cells ($\eta_\mathrm{eff} = 0.14\,\mathrm{N\,s\,m^{-1}} \pm 0.05$ SD), which confirms the detachment of the cortex from the membrane in silenced cells.

5. Conclusion

We probe the attachment of the cytoskeleton to the membrane by using dynamical aspiration experiments and geometrical measurements of the amount of the aspirated membrane and cytoskeleton. We show that the attachment is weakened in cells lacking the B9 domain protein compared to wild-type cells. We provide an estimate of the coefficient that characterizes the friction between the cytoskeleton and the membrane. In general, these experiments bring an alternative to static experiments [13, 18] where the adhesion energy is derived. In *Paramecium*, like in other motile organisms, static experiments are technically unfeasible due to the high pressure that needs to be applied to avoid cell escape, like in our study. Such a biophysical approach in a living organism in its natural environment allows addressing fundamental biological questions about the link between the lack of a gene, the cell behavior and the underlying mechanics.

Acknowledgments

CC acknowledges financial support from the Association pour la Recherche contre le Cancer. This work was supported by the ANR ‘Programme Blanc’ (ANR-08-BLAN-0012–12) and SYSCOM (ANR-08-SYSC-013–03). PD-W acknowledges financial support from Genopole (ATIGE ‘Centriole and associated pathologies’).

References

[1] Dowdle W E *et al* 2011 Disruption of a ciliary B9 protein complex causes Meckel syndrome *Am. J. Hum. Genet.* **89** 94–110

[2] Town T *et al* 2008 The stumpy gene is required for mammalian ciliogenesis *Proc. Natl Acad. Sci. USA* **105** 2853–8

[3] Weatherbee S D, Niswander L A and Anderson K V 2009 A mouse model for Meckel syndrome reveals Mks1 is required for ciliogenesis and Hedgehog signaling *Hum. Mol. Genet.* **18** 4565–75

[4] Breunig J J, Sarkisian M R, Arellano J I, Morozov Y M, Ayoub A E, Sojitra S, Wang B, Flavell R A, Rakic P and Town T 2008 Primary cilia regulate hippocampal neurogenesis by mediating sonic hedgehog signaling *Proc. Natl Acad. Sci. USA* **105** 13127–32

[5] Dawe H R *et al* 2007 The Meckel–Gruber syndrome proteins MKS1 and meckelin interact and are required for primary cilium formation *Hum. Mol. Genet.* **16** 173–86

[6] Tammachote R *et al* 2009 Ciliary and centrosomal defects associated with mutation and depletion of the Meckel syndrome genes MKS1 and MKS3 *Hum. Mol. Genet.* **18** 3311–23

[7] Bialas N J *et al* 2009 Functional interactions between the ciliopathy-associated Meckel syndrome 1 (MKS1) protein and two novel MKS1-related (MKSR) proteins *J. Cell Sci.* **122** 611–24

[8] Pomel S, Diogon M, Bouchard P, Pradel L, Ravet V, Coffe G and Vigues B 2006 The membrane skeleton in Paramecium: molecular characterization of a novel epiplasmin family and preliminary GFP expression results *Protist* **157** 61–75

[9] Kissmehl R, Sehring I, Wagner E and Plattner H 2004 Immunolocalization of actin in *Paramecium* cells *J. Histochem. Cytochem.* **52** 1543–59

[10] Williams C L, Winkelbauer M E, Schafer J C, Michaud E J and Yoder B K 2008 Functional redundancy of the B9 proteins and nephrocystins in *Caenorhabditis elegans* ciliogenesis *Mol. Biol. Cell* **19** 2154–68

[11] Sheetz M P 2001 Cell control by membrane–cytoskeleton adhesion *Nature Rev. Mol. Cell Biol.* **2** 392–6

[12] Sit P S, Spector A A, Lue A J C, Popel A S and Brownell W E 1997 Micropipette aspiration on the outer hair cell lateral wall *Biophys. J.* **72** 2812–9

[13] Merkel R, Simson R, Simson D A, Hohenadl M, Boulbitch A, Wallraff E and Sackmann E 2000 A micromechanic study of cell polarity and plasma membrane cell body coupling in Dictyostelium *Biophys. J.* **79** 707–19

[14] Allen R D 1971 Fine structure of membranous and microfibrillar systems in the cortex of *Paramecium caudatum J. Cell Biol.* **49** 1–20

[15] Sehring I M, Reiner C, Mansfeld J, Plattner H and Kissmehl R 2007 A broad spectrum of actin paralogs in *Paramecium tetraurelia* cells display differential localization and function *J. Cell Sci.* **120** 177–90

[16] Guevorkian K and Valles J M 2006 Swimming *Paramecium* in magnetically simulated enhanced, reduced, and inverted gravity environments *Proc. Natl Acad. Sci. USA* **103** 13051–6

[17] Hamel A, Fisch C, Combettes L, Dupuis-Williams P and Baroud C N 2011 Transitions between three swimming gaits in *Paramecium* escape *Proc. Natl Acad. Sci. USA* **108** 7290–5

[18] Oghalai J S, Patel A A, Nakagawa T and Brownell W E 1998 Fluorescence-imaged microdeformation of the outer hair cell lateral wall *J. Neurosci.* **18** 48–58

[19] Brugués J, Maugis B, Casademunt J, Nassoy P, Amblard F and Sens P 2010 Dynamical organization of the cytoskeletal cortex probed by micropipette aspiration *Proc. Natl Acad. Sci. USA* **107** 15415–20

[20] Evans E and Needham D 1987 Physical properties of surfactant bilayer membranes: thermal transitions, elasticity, rigidity, cohesion, and colloidal interactions *J. Phys. Chem.* **91** 4219–28

[21] Dimova R, Aranda S, Bezlyepkina N, Nikolov V, Riske K A and Lipowsky R 2006 Apractical guide to giant vesicles. Probing the membrane nanoregime via optical microscopy *J. Phys.: Condens. Matter* **18** S1151–S76